

# ULRR

## The Effect of pendent groups upon flexibility in coordination networks with square lattice topology

Item Type	Article
Authors	Li, Xia;Sensharma, Debobroto;Koupepidou, Kyriaki;Kong, Xiang-Jing;Zaworotko, Michael
Citation	ACS Materials Letters 5(9), pp. 2567–2575
Publisher	American Chemical Society
Download date	2026-06-11 11:10:54
Item License	<a href="https://creativecommons.org/licenses/by-nc-sa/4.0/">https://creativecommons.org/licenses/by-nc-sa/4.0/</a>
Link to Item	<a href="https://doi.org/10.34961/researchrepository-ul.24182427">https://doi.org/10.34961/researchrepository-ul.24182427</a>

# The Effect of Pendent Groups upon Flexibility in Coordination Networks with Square Lattice Topology

Xia Li, Debobroto Sensharma, Kyriaki Koupepidou, Xiang-Jing Kong, and Michael J. Zaworotko\*

Cite This: *ACS Materials Lett.* 2023, 5, 2567–2575

Read Online

ACCESS |



Metrics &amp; More

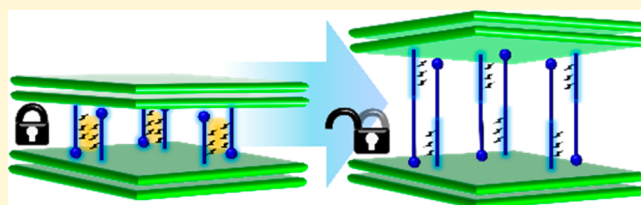


Article Recommendations



Supporting Information

**ABSTRACT:** Gas or vapor-induced phase transformations in flexible coordination networks (CNs) offer the potential to exceed the performance of their rigid counterparts for separation and storage applications. However, whereas ligand modification has been used to alter the properties of such stimulus-responsive materials, they remain understudied compared with their rigid counterparts. Here, we report that a family of  $\text{Zn}^{2+}$  CNs with square lattice (sql) topology, differing only through the substituents attached to a linker, exhibit variable flexibility. Structural and  $\text{CO}_2$  sorption studies on the sql networks,  $[\text{Zn}(\text{S-Ria})(\text{bphy})]_n$ , ia = isophthalic acid, bphy = 1,2-bis(pyridin-4-yl)hydrazine,  $\text{R} = -\text{CH}_3$ ,  $-\text{OCH}_3$ ,  $-\text{C}(\text{CH}_3)_3$ ,  $-\text{N}=\text{N}-\text{Ph}$ , and  $-\text{N}=\text{N}-\text{Ph}(\text{CH}_3)_2$ , 2–6, respectively, revealed that the substituent moieties influenced both structural and gas sorption properties. Whereas 2–3 exhibited rigidity, 4, 5, and 6 exhibited reversible transformation from small pore to large pore phases. Overall, the insight into the profound effect of pendent moieties of linkers upon phase transformations in this family of layered CNs should be transferable to other CN classes.



Flexible coordination networks (CNs), also known as flexible metal–organic frameworks (FMOFs),<sup>1–5</sup> are an emerging subset of CNs<sup>6,7</sup> that can undergo stimuli-induced phase transformations. When the external stimulus is gas or vapor pressure, reversible transformation(s) between low- and high-porosity phases can occur, resulting in stepped sorption isotherm profiles with characteristic adsorbate pressure above a threshold or “gate-opening” pressure ( $P_{\text{GO}}$ ).<sup>8</sup> Such isotherms can exhibit enhanced working capacities compared with the type I (Langmuir) sorption isotherms typically displayed by rigid materials. Therefore, FMOFs are of potential utility in gas storage<sup>9–12</sup> or separation<sup>13–16</sup> and water sorption.<sup>17,18</sup>

Unfortunately, control over the properties of FMOFs is still a challenge. Whereas >118000 entries have been archived in the metal–organic framework (MOF) subset of the Cambridge Structural Database (CSD),<sup>19</sup> the number of reported FMOFs is much smaller.<sup>3,4</sup> Nevertheless, that FMOFs can exhibit strong performance for gas/vapor storage or separation makes elucidation of crystal engineering principles for the design of FMOFs a topical area of investigation. The mechanism of flexibility in FMOFs tends to belong to one or more of the following three categories:<sup>3,4</sup> ligand contortion (e.g., bending, twisting, and/or rotation);<sup>18,20–23</sup> structural changes in the metal node or molecular building block (MBB)<sup>24</sup> coordination environment (e.g., deformation, iso-

merism, or changes in coordination number);<sup>21,23,25–27</sup> relative motions of individual nets (such as interpenetrated or layered net sliding or expansion).<sup>16,28,29</sup> There also exist examples of light-modulated adsorbents with photoactive linkers.<sup>30–32</sup>

A strategy to obtain FMOFs involves use of flexible linkers to construct FMOFs.<sup>20,33,34</sup> In this context, tuning the flexibility of a parent CN through elongation of the backbone or side chain of a linker can enhance flexibility.<sup>35–37</sup> For example, Kaskel’s group reported the flexible three-dimensional (3D) materials **DUT-49** and **DUT-50**, wherein increasing ligand length led to enhanced flexibility in the resulting frameworks.<sup>38,39</sup> Alkyl anhydride side-chains on linkers altered the flexibility of **DMOF-1-NH<sub>2</sub>** derivatives, as reported by Cohen’s group.<sup>40</sup> Webley’s group reported that replacing the rigid BPY (4,4’-bipyridine) linker in **Zn(BPDC)**-(BPY) to the flexible BPP (1,3-bis(4-pyridyl)-propane) analogue in **Zn(BPDC)(BPP)** through postsynthetic ligand exchange induced flexibility.<sup>41</sup> Collectively, these reports

Received: May 29, 2023

Accepted: August 2, 2023

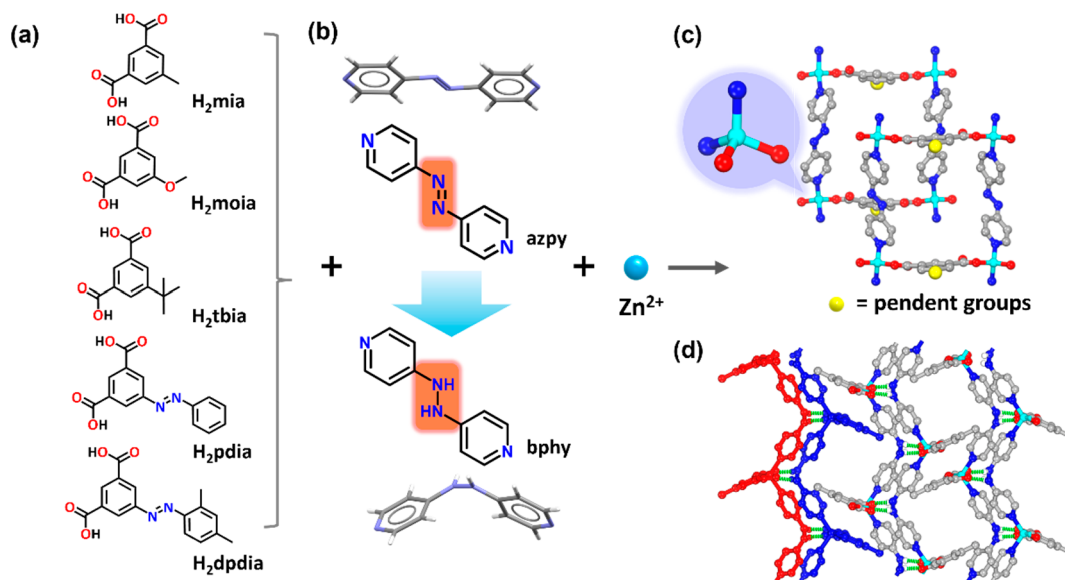


**Figure 1.** (a) The five functionalized isophthalic acid (ia) ligands studied herein: 5-methylisophthalic acid ( $H_2mia$ ); 5-methoxyisophthalic acid ( $H_2moia$ ); 5-(*tert*-butyl)isophthalic acid ( $H_2tbia$ ); (*E*)-5-(phenyldiazenyl)isophthalic acid ( $H_2pdia$ ); and (*E*)-5-((2,4-dimethylphenyl)diazenyl)isophthalic acid ( $H_2dpdia$ ). (b) *In situ* reduction of 1,2-di(pyridin-4-yl)diazene (azpy) to 1,2-bis(pyridin-4-yl)hydrazine (bphy) occurred during the synthesis of sql topology CNs. (c) The tetrahedral coordination environment of the zinc cations in the CNs studied herein. (d) Interlayer hydrogen bonds (green dashed line) connect two sql layers (red, blue) to form bilayers; crystal packing of these bilayers is directed by interdigitation (partial hydrogen atoms omitted for clarity).

highlight how pendent groups or ligand extensions can induce flexibility in CNs.<sup>42–45</sup>

CNs that can exhibit subnetwork motion generally exhibit phase transformations involving noncovalent bonds between subnetworks induced via guest inclusion. In the case of two-dimensional (2D) CNs, interlayer expansion can enable adsorption and desorption at gas pressures above and below threshold pressure, respectively. Representative examples include CNs of the elastic layer-structured metal–organic framework (ELM) family with square lattice or sql topology.<sup>28,33,46–49</sup> Such structures have relatively weak interactions between the layers, meaning that solvent- or gas-induced expansion can be relatively facile. Such sql interlayer expansions are sometimes associated with switching, i.e., transformation from nonporous to porous phases over a narrow pressure range. Void volume changed from 0 to 65.2% in the ELM material sql-1-Co-NCs.<sup>16</sup> However, the reliance of ELMs on a specific structural blueprint (metal nodes, counteranions, and linear pyridine ligands) limits their compositional diversity. A strategy to obtain sql topology FMOFs with greater diversity involves different linkers; a switching sql CN composed of two linkers and Ni(II) cations, sql-(azpy)(pdia)-Ni, was recently reported by our group. Regulated by interlayer H-bonds, slippage between adjacent sql layers was enabled by the contortion of the pendent ligand (*E*)-5-(phenyldiazenyl)isophthalic acid ( $H_2pdia$ ).<sup>18</sup>

Here, we present a new crystal engineering strategy to establish control over expansion between sql layers, varying the bulk and length of pendent groups in a family of isophthalic acid linkers. The prototypal structure of this family of networks,  $[Zn(nipa)(bphy)]_n$ , **1**, was previously reported by Chen's group and is comprised of  $Zn^{2+}$  nodes, 5-nitroisophthalic acid ( $H_2nipa$ ) and 1,2-bis(pyridin-4-yl)hydrazine (bphy).<sup>50</sup> That the 5-substituted isophthalate moiety is tunable enables a family of related CNs to be generated by varying the length and steric bulk of the ia substituents. The shorter ia

linkers containing methyl, methoxy, and *tert*-butyl groups are available commercially and have been used extensively to generate CNs, with 353, 139, and 212 hits, respectively, archived in the CSD (version 5.43, November 2022).<sup>51</sup> The bulkier ia substituents studied herein, phenyldiazenyl and (2,4-dimethylphenyl)diazenyl, were obtained by the Wallach reaction,<sup>52</sup>  $H_2pdia$  and (*E*)-5-((2,4-dimethylphenyl)diazenyl)isophthalic acid ( $H_2dpdia$ ) being synthesized in gram scale. Thus far, only 5 and 2 CNs based upon  $H_2pdia$  and  $H_2dpdia$ , respectively, are archived in the CSD. One pdia CN was studied for gas- and vapor-induced flexibility,<sup>18</sup> whereas two were studied for light-modulated flexibility.<sup>53,54</sup> Five new sql CNs comprised of  $Zn^{2+}$ , 1,2-bis(pyridin-4-yl)hydrazine (bphy) linkers, and functionalized isophthalic acid linkers:  $[Zn(mia)(bphy)]_n$  (**2**, mia = 5-methylisophthalate),  $[Zn(moia)(bphy)]_n$  (**3**, moia = 5-methoxyisophthalate),  $[Zn(tbia)(bphy)]_n$  (**4**, tbia = 5-(*tert*-butyl)isophthalate),  $[Zn(pdia)(bphy)]_n$  (**5**, pdia = (*E*)-5-(phenyldiazenyl)isophthalate), and  $[Zn(dpdia)(bphy)]_n$  (**6**, dpdia = (*E*)-5-((2,4-dimethylphenyl)diazenyl)isophthalate) were prepared, enabling us to study the effect of pendent group substitution upon the flexibility of the CNs.

**Synthesis and structural analysis.** Single crystals of **2–6** were prepared by solvothermal reaction of zinc(II) nitrate,  $H_2(R)ia$  (5-(*R*)isophthalic acid, *R* = methyl, methoxy, *tert*-butyl, phenyldiazenyl, and 2,4-dimethylphenyldiazenyl, Figure 1a), and azpy ((*E*)-1,2-di(pyridin-4-yl)diazene, Figure 1b) dissolved in *N,N*-dimethylformamide (DMF) and 0.1 M aqueous sodium hydroxide for **2**, **5**, and **6**, or water for **3** and **4**, at 105 °C. Single-crystal X-ray diffraction (SCXRD) studies of the as-synthesized crystals **2–6** revealed that **2**, **3**, and **6** had crystallized in  $P2_1/n$ , **4- $\alpha'$**  and **4- $\beta'$**  in  $P2_1$ , and **5** in  $P2_12_12$  (Figure 1c, Table S1). As previously reported for **1**, azpy underwent *in situ* reduction to bphy during synthesis (Figure 1b).<sup>55</sup> The mononuclear, tetrahedral molecular building blocks (MBBs)<sup>24</sup> of **2–6** are comprised of  $Zn^{2+}$  cations coordinated to two N-donor atoms from two

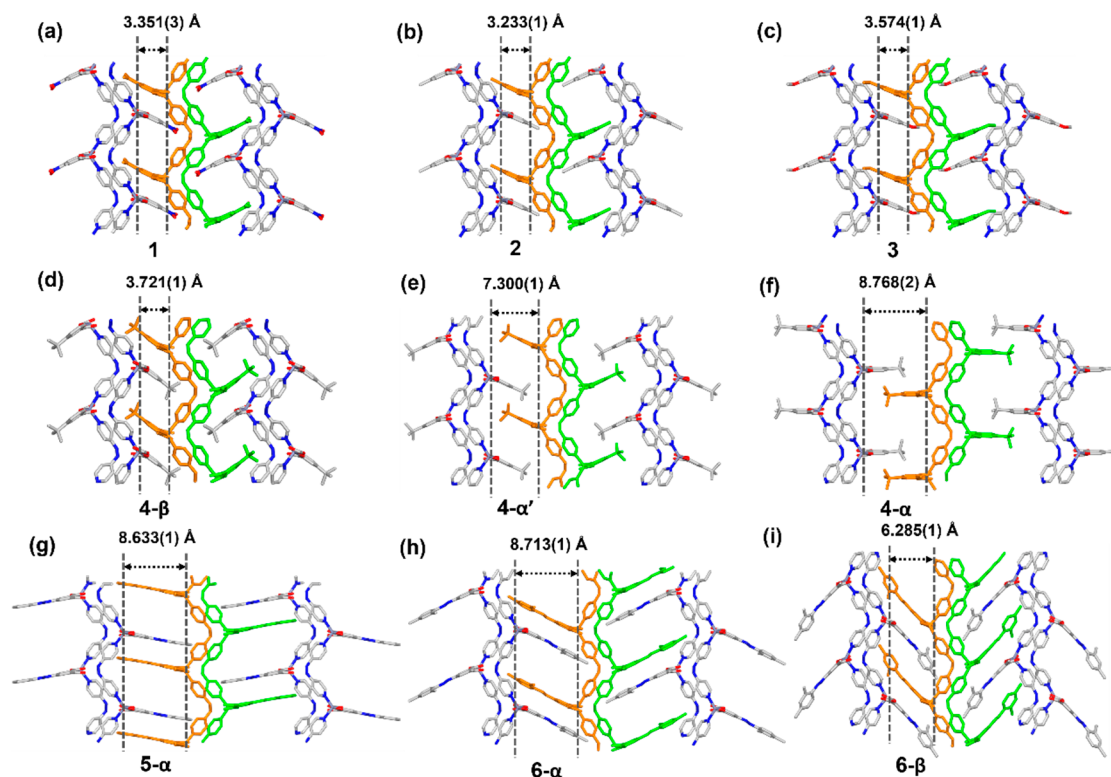


**Figure 2.** Perpendicular distances between *sql* planes (as defined by three adjacent  $\text{Zn}^{2+}$  centers in the same *sql* layer) across channels in (a) 1, (b) 2, (c) 3, (d) narrow-pore phase 4- $\beta$ , (e) intermediate phase 4- $\alpha'$ , (f) open phase 4- $\alpha$ , (g) open phase 5- $\alpha$ , (h) open phase 6- $\alpha$ , and (i) narrow-pore phase 6- $\beta$  (hydrogen atoms are omitted for clarity).

separate bphy ligands and two monodentate carboxylate O-donor atoms from separate isophthalate ligands. The general formula for this family of compounds is  $[\text{Zn}((\mathbf{R})\text{ia})(\text{bphy})]_n$  ( $\mathbf{R}$  = methyl, methoxy, *tert*-butyl, phenyldiazanyl, and 2,4-dimethylphenyldiazanyl, Figure 1a,c). 2-6 each exhibit layered structures with *sql* topology, the square comprised of bphy ligands and parallel isophthalate moieties that form the edges of a quadrilateral with  $\text{Zn}^{2+}$  centers at the vertices. Interlayer hydrogen bonds were observed in all five materials between hydrazine hydrogen atoms in bphy from one *sql* layer and the uncoordinated oxygen atom in an isophthalate ligand from an adjacent *sql* layer, lengths ranging from  $d_{\text{N}\cdots\text{O}} = 2.799(5)$  Å in 2 to 2.849(12) Å in 4- $\alpha$  (Table S2). These H-bonding interactions enabled the *sql* layers to form bilayers with pendent groups extending orthogonally in opposite directions. The pendent groups interdigitate with adjacent H-bonded bilayers to form a porous structure (Figure 1d). Under the same synthetic conditions used for 2-6, isophthalic acid (ia) did not yield the same bilayer structure (Figure S1).

The pendent moieties influence the pore dimensions of each compound, with 1-6 exhibiting different guest-accessible void volumes in their as-synthesized structures (denoted as - $\alpha$ , Figure S2). While retaining the same topology and bilayer architecture, the steric bulk of these five pendent groups resulted in pores of different dimensions. Disordered solvent in the pores were not modeled during structure refinement; a solvent mask<sup>56</sup> was applied. The guest-accessible void spaces calculated by PLATON<sup>57</sup> in 1, 2, 3, 4- $\alpha$ , 5- $\alpha$ , and 6- $\alpha$  were 21.6%, 22.5%, 23.9%, 45.4%, 40.5%, and 35.7%, respectively (Figure S2). An incongruence of incremental guest-accessible void space was observed in 4- $\alpha$ , which was caused by the large volume of the relatively short *tert*-butyl group, which allowed

the inclusion of additional guests in the gap between the *tert*-butyl group and the adjacent *sql* plane. In the other five compounds, spaces of this type were not observed between the terminal group and adjacent *sql* layers. The bulk purity of each as-synthesized phase was confirmed by powder X-ray diffraction (PXRD) through comparison with the PXRD pattern calculated from the corresponding SCXRD structure (Figure S3).

**Activation.** Activation was conducted by heating to 333 K under a vacuum after performing solvent exchange using dichloromethane (DCM). 1, 2, and 3 did not show any appreciable change in their crystal structures as determined by PXRD (Figure S3). However, 4-6 showed marked PXRD pattern changes because of phase transformation to low-porosity “- $\beta$ ” phases, 4- $\beta$ , 5- $\beta$ , and 6- $\beta$ , respectively. Notably, upon heating without solvent exchange at 343 K for 30 min, 4- $\alpha$  transformed to a partially solvated phase with intermediate porosity, 4- $\alpha'$ , while 5 and 6 did not show corresponding intermediate phases.

The relative bulk of the ia ligands with pendent groups was evaluated by the SCXRD determined distance between the C atom at the 5- position of ia and the terminal O (1) or H atom (2-6) of the pendent moiety. Distances were found to be 2.318(4) Å for nipa<sup>2-</sup>, 2.060(3) Å for mia<sup>2-</sup>, 3.180(2) Å for moia<sup>2-</sup>, 3.354(6) Å for tbia<sup>2-</sup>, 7.228(3) Å for pdia<sup>2-</sup>, and 8.099(5) Å for dpdia<sup>2-</sup> (Figure S4).

Analysis of the SCXRD structures revealed that 1-3 and 4- $\beta$  are isomorphous, their unit cell volumes being 2162.87, 2137.5(3), 2227.66(17), and 2270.2(2) Å<sup>3</sup>, respectively (Table S1). That 4- $\beta$  is comprised of a bulkier ligand (tbia<sup>2-</sup>) means that it exhibits cavities with voids of 12.4%, while 1-3 have pores with voids of 21.6%, 22.5%, and 23.9%, respectively

(Figures S2 and S5). Among these four compounds, only **4** was found to exhibit solvent-triggered phase changes involving clay-like **sql** bilayer expansion, resulting in three distinct phases, **4-β**, **4-α'**, and **4-α**. In contrast, the structures of **1-3** were unaffected by activation (Table S1).

Further structural analysis revealed that, in **1-3**, the edge lengths of the squares comprising the **sql** square lattice Zn-to-Zn distances are 10.185(1) and 11.104(1) Å in **1**, 10.189(1) and 11.199(1) Å in **2**, and 10.211(7) and 11.106(8) Å in **3**, along the isophthalate-bridged edge and the bphy-bridged edge, respectively (Table S3). The torsion angles between the pyridyl carbons (at the 4-position) and hydrazine N atoms ( $\angle\text{C-N-N-C}$ ) in bphy are 95.9(3)° for **1**, 99.7(5)° for **2**, and 96.3(5)° for **3**. The dihedral angles in  $\text{mia}^{2-}$  between each carboxyl plane and the aromatic ring plane of the isophthalate moieties are 9.0(2)° and 18.5(2)° for **1**, 10.6(3)° and 20.4(3)° for **2**, and 6.5(4)° and 16.6(3)° for **3**. The perpendicular distances between two **sql** planes (defined by three adjacent  $\text{Zn}^{2+}$  centers in the same **sql** layer) are 3.351(1), 3.233(1), and 3.574(1) Å in **1-3**, respectively (Figure 2a–c).

The interlayer separation for the closed phase of **4**, 3.721(1) Å, changed dramatically to 7.300(1) Å in **4-α'** and 8.768(2) Å in **4-α** (Figure 2d,e). **4-α**, **4-α'**, and **4-β** exhibited cell volumes of 3415.6(5), 3068.09(18), and 2270.2(2) Å<sup>3</sup> (Table S1). The guest-accessible space was determined to be 45.4% in **4-α** and 36.9% in **4-α'**, while in **4-β** it was only 12.4% (Figure S5). To adapt to the effect of desolvation, bphy and  $\text{tbia}^{2-}$  displayed flexibility in two dimensions, within and outside of the **sql** plane. Within the **sql** plane, following the phase change from **4-α** to **4-α'** to **4-β**, the edge length between ia-bridged  $\text{Zn}^{2+}$  cations increased from 10.152(2) to 10.203(1) to 10.252(1) Å, while that between bphy-bridged  $\text{Zn}^{2+}$  cations decreased from 11.349(2) to 11.209(1) to 11.021(1) Å (Table S3). In each **sql** square lattice, the bphy linker exhibited flexibility with a change in the torsion angle about the hydrazine moiety ( $\angle\text{C-N-N-C}$ ) from 101.9(10)° to 98.3(5)° to 89.2(7)°, in **4-α** to **4-α'** to **4-β** (Table S3). Hinge-like deformations of the pendent isophthalate linker were also evident, with the dihedral angle between the carboxyl plane and the isophthalate aromatic ring plane being enlarged from 6.4(8)/10.2(1)° to 9.7(3)/21.2(3)° and from 11.4(5)/27.6(4)° in **4-α** to **4-α'** to **4-β**, respectively (Table S3).

Compared with **1-4**, longer pendent moieties are present in **5** and **6** (Figure S4). Crystal fragmentation upon desolvation of **5-α**, as shown in scanning electron microscopy (SEM) images (Figure S6), precluded SCXRD analysis of the activated phase, **5-β**. Nevertheless, PXRD studies on **5** indicated a transformation similar to that observed for **6** (Figure S3), for which SCXRD analysis of the activated phase, **6-β**, was feasible. The SCXRD structures of **6** showed that the pore shape changed from the guest-accessible channels present in **α** to isolated cavities in the **β** phase, as also seen in **4**. The guest-accessible space in **6-α** was determined to be 35.7%, whereas that in **6-β** was 16.4% (Figure S5). However, even though the structural flexibility of **4** was facilitated by the bulky  $\text{tbia}^{2-}$  moiety, it was a hinge-like motion of pendent moieties  $\text{dpdia}^{2-}$  in **6** that dominated the expansion between adjacent **sql** bilayers. During the phase transformation from **6-α** to **6-β**, the hinge-like motion is evidenced by a change in the dihedral angles of the carboxyl plane and the isophthalate aromatic ring plane: 8.4(4)/22.8(4)° in **6-α** and 18.1(4)/29.8(4)° in **6-β** (Table S3). Furthermore, additional twisting of the  $\text{dpdia}^{2-}$  ligand was observed around the azo bond, with the dihedral angle

between the isophthalate aromatic ring plane and *m*-xylyl aromatic ring varying from 5.2(3)° to 31.7(4)° in **6-α** and **6-β**, respectively (Table S3). Therefore, the diazo moiety can be an additional source of structural flexibility in **6** compared to **4**. Triggered by solvent molecules, this linker deformation of  $\text{dpdia}^{2-}$  in **6** resulted in a decrease of the perpendicular distances between two **sql** planes (defined by three adjacent  $\text{Zn}^{2+}$  centers in the same **sql** layer), with distances of 8.713(1) Å in **6-α** and 6.285(1) Å in **6-β** (Figure 2h,i). **1-6** can therefore be classified into two groups by the effect of the various side chains incorporated into each structure. The materials with bulkier (**4**) or longer (**5** and **6**) side chains exhibited flexible behavior, with **5** and **6** containing an additional flexible element, the diazo moiety, which can induce hinge-like motion and further facilitate **sql** bilayer expansion. **1-3** did not exhibit layer contraction.

**Analysis of flexibility.** Further analysis of the as-synthesized phases indicated that noncovalent interactions between isophthalate moieties in neighboring **sql** layers play a role in regulating the flexibility of each framework (Figure 3a–d). In

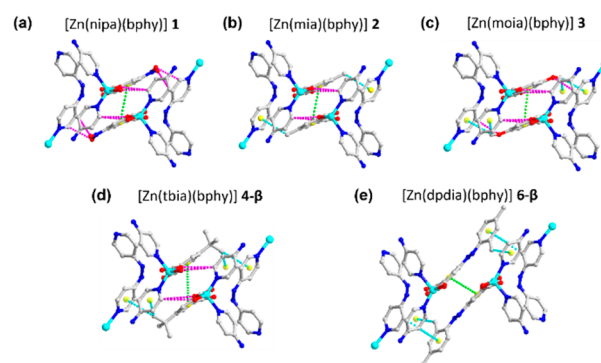


**Figure 3.** Noncovalent interactions between adjacent **sql** layers with highlighted  $\pi\cdots\pi$  in green dashed lines,  $\text{C-H}\cdots\pi$  interactions in blue dashed lines, and  $\text{C-H}\cdots\text{O}$  interactions in magenta dashed lines in (a) **1**, (b) **2**, (c) **3**, (d) **4-β**, and (e) **6-β**. (Zn, O, N, C, and created centroid atoms are represented by light blue, red, dark blue, gray, and yellow, respectively. Hydrogen atoms are omitted for clarity.)

the isomorphous structures **1** & **2** and **3** & **4-β**,  $\pi\cdots\pi$ ,  $\text{C-H}\cdots\pi$ , and  $\text{C-H}\cdots\text{O}$  interactions exist (Table S4). Specifically, a  $\pi\cdots\pi$  interaction in each phase was exhibited by a pair of offset-stacked isophthalate rings from adjacent **sql** layers, with  $d_{\text{Centroid}\cdots\text{Centroid}} = 4.137(4)$  Å in **1**, 4.176(1) Å in **2**, 3.811(1) Å in **3**, and 4.256(2) Å in **4-β**.  $\text{C-H}\cdots\pi$  interactions from the terminal C atom of isophthalate linkers and a pyridyl ring of bphy linkers were found in **2**, **3**, and **4-β**, with average distances of  $d_{\text{C}\cdots\text{Centroid}} = 3.543$ , 3.564, and 3.745 Å, respectively. Additionally,  $\text{C-H}\cdots\text{O}$  interactions were also observed in all four compounds. In **1**, **2**, **3**, and **4-β**, four, two, three, and four pairs of  $\text{C-H}\cdots\text{O}$  interactions were found with average distances  $d_{\text{C}\cdots\text{O}}$  of 3.195, 3.283, 3.448, and 3.740 Å, respectively. When comparing the distances of the three types of noncovalent interactions measured in **1-3** vs **4-β**, **4-β** was found to exhibit longer distances, indicative of a relative weakening of noncovalent interactions. These weaker interactions might explain why guest-triggered **sql** interlayer motion was observed in **4** but not in **1-3**.

The presence of bulkier substituents in **5** and **6** impacts noncovalent interactions between pairs of **sql** layers that define

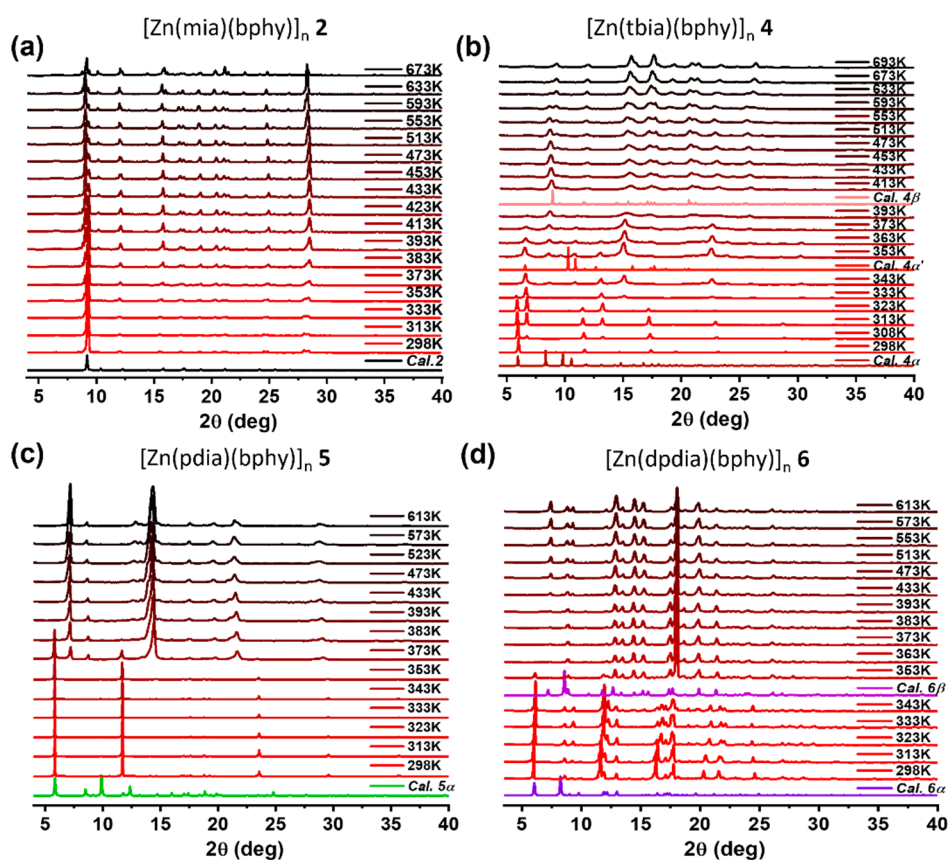


**Figure 4.** Variable-temperature PXRD patterns of (a) **2** from 298 to 673 K, (b) **4** from 298 to 613 K, (c) **5** from 298 to 613 K, and (d) **6** from 298 to 613 K under  $N_2$  atmosphere and comparison with calculated PXRD patterns from their SCXRD determined structures.

the channels in their respective  $\beta$  phases (Table S4). Since similar lengths of longer pendent moieties are found in **5** and **6**, 7.228(3) Å for  $pdia^{2-}$  and 8.099(5) Å for  $dpdi^{2-}$ , respectively (Figure S4), and the PXRD patterns of **5** and **6** are similar, **5** was expected to be amenable to transformation like **6**. In **6- $\beta$** , although pairwise stacking between isophthalate moieties in neighboring **sql** layers was observed, the moieties present in the side chains played a more active role in determining the crystal packing. A  $\pi \cdots \pi$  interaction between a pair of offset stacked isophthalate rings of  $dpdi^{2-}$  ligands from adjacent **sql** layers with distances of  $d_{C_{\text{Centroid}} \cdots C_{\text{Centroid}}} = 3.825(1)$  Å and C–H $\cdots\pi$  interactions between *m*-xylyl moieties and bphy pyridyl rings, with distances of  $d_{C \cdots C_{\text{Centroid}}} = 4.110(6)$ , 4.214(5), and 4.271(7) Å, were observed (Figure 3e). Notably, most of the average distances associated with  $\pi \cdots \pi$ , C–H $\cdots\pi$ , and C–H $\cdots$ O interactions in **4- $\beta$**  (4.256, 3.745, and 3.740 Å) and **6- $\beta$**  (3.825, 4.198 Å, C–H $\cdots$ O interaction was not observed) are longer than the corresponding distances in **1** (4.137 and 3.195 Å, C–H $\cdots\pi$  was not observed), **2** (4.176, 3.543, and 3.283 Å), and **3** (3.811, 3.564, and 3.448 Å). Considering the observation of weaker interactions in **4- $\beta$**  and **6- $\beta$**  along with the denser packing of **sql** layers in **1**, **2**, and **3**, we postulate that **4-6** are more amenable to structural transformation upon solvent removal than **1-3**.

**Thermal and Fourier Transform Infrared (FTIR) analysis.** To gain insight into the phase transformations, variable-temperature PXRD (VT-PXRD) tests under a  $N_2$  atmosphere were conducted on as-synthesized samples of **1-6**. During the temperature ramping process, **1**, **2**, and **3** did not exhibit significant peak shifting, and their respective PXRD patterns

calculated from their SCXRD structures matched well with experimental data (Figures 4a and S7). **4** exhibited three distinct PXRD patterns. As shown in Figure 4b, the experimental VT-PXRD patterns at 298, 353, and 413 K match well with the calculated PXRD patterns from the SCXRD-determined structures **4- $\alpha$** , **4- $\alpha'$** , and **4- $\beta$** , respectively (intensity variations could be caused by preferred orientation or different guests, Figure S8). **5** and **6** each exhibited two PXRD patterns in their VT-PXRD data. The experimental PXRD patterns of the as-synthesized phases at 298 K match well with the calculated PXRD patterns from the respective SCXRD structures of **5- $\alpha$**  and **6- $\alpha$**  (Figures 4c,d and S8). When the temperature was increased to 353 K, a PXRD pattern matching the calculated structure of **6- $\beta$**  was observed (Figure 4f). A similar change was observed from **5- $\alpha$**  at 373 K; however, in the absence of SCXRD data for **5- $\beta$** , its structure cannot be directly compared to **5- $\alpha$** . Thermogravimetric analysis (TGA) revealed gradual weight losses of 12.5% and 11.3% for **2** and **3** from 100 to 150 °C, corresponding to four and three water molecules, respectively, per formula unit (weight losses calculated from SCXRD data are 14.3% and 10.8%, respectively). TGA conducted on **4-6** showed 46%, 24%, and 21% weight loss from 120 to 150 °C, corresponding to three DMF molecules in **4**, two DMF molecules in **5** and **6** per formula, respectively (Figure S9). Weight loss above the respective phase-change threshold temperatures can be attributed to framework decomposition occurring above the temperature range covered in VT-PXRD experiments. The presence of guests in the pores of **1-6** was also studied by FTIR spectroscopy. FTIR studies of the as-synthesized forms of **1-3**

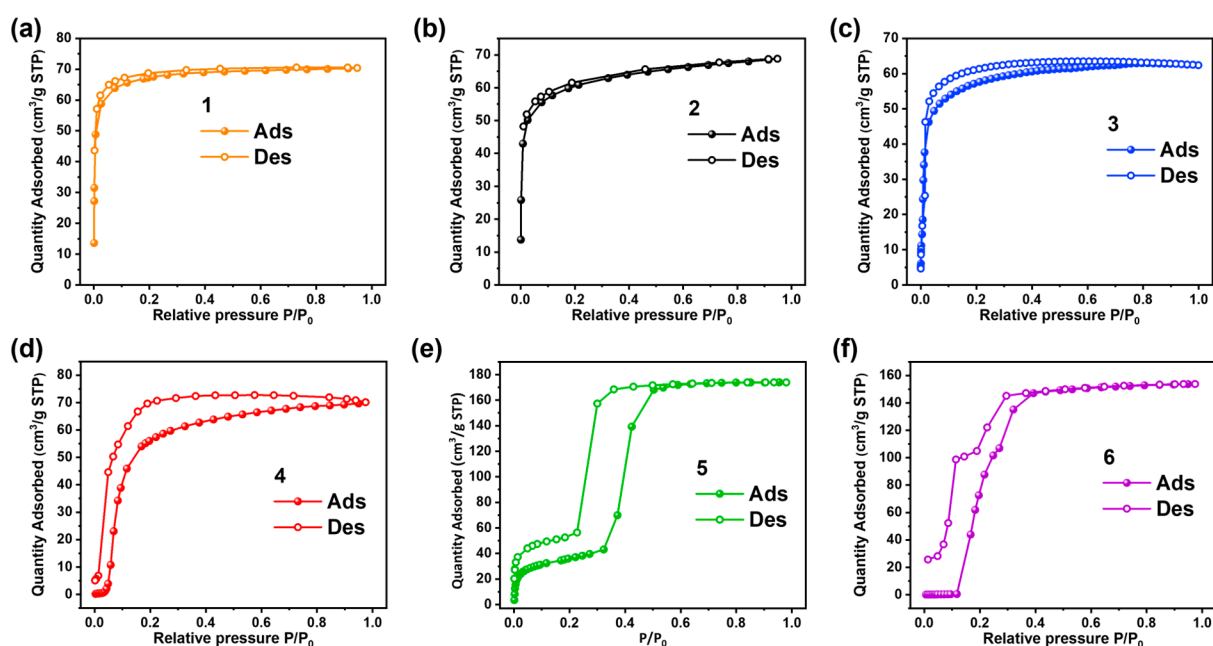


Figure 5. CO<sub>2</sub> sorption isotherm at 195 K of (a) 1, orange; (b) 2, black; (c) 3, blue; (d) 4, red; (e) 5, green; and (f) 6, purple. Adsorption and desorption branches are indicated by solid and open symbols, respectively.

indicated the presence of water (O–H stretching at 3369, 3447, and 3452 cm<sup>-1</sup>). In 4–6, C=O stretching bands from DMF were detected at 1677, 1672, and 1663 cm<sup>-1</sup> (Figure S10).

**Gas sorption.** Since the phase transformations in 4–6 can be induced by immersion in liquid solvents, we anticipated that gases might also trigger phase transformation(s). CO<sub>2</sub> isotherms were collected at 195 K to investigate adsorption characteristics since CO<sub>2</sub> possesses a small kinetic diameter (3.30 Å) and typically exhibits relatively strong sorbent–sorbate interactions vs N<sub>2</sub> and Ar. CO<sub>2</sub> therefore tends to trigger gate opening at 195 K and provide access to the full  $P/P_0$  range from 0 to 1.<sup>58</sup> Sorption experiments conducted on the activated samples of 1–6 indicated that 1–3 showed type I isotherms characteristic of rigid microporous materials (Figure 5a–c). Conversely, 4–6 exhibited stepped isotherms consistent with phase transformations. The CO<sub>2</sub> uptakes of 1–3 at 1 bar and 195 K were determined to be 70, 69, and 62 cm<sup>3</sup>/g with pore sizes of 4.12, 4.16, and 4.11 Å, respectively (Figure S11). In 4 and 6, “closed-to-open” switching (Type F–IV) isotherms at characteristic gate-opening pressures ( $P_{GO}$ ) were observed at  $P_{GO} = 0.04$  and 0.12 bar (Figures 5d,f and S12). In 5, an “open-to-more open” step or Type F–II isotherm was observed at  $P_{GO} = 0.33$  bar (Figures 5e and S12). The differences in types of sorption isotherms indicate that a degree of porosity was preserved in the narrow pore phase of 5 after activation, while nonporous phases were obtained in 4 and 6 after activation. The CO<sub>2</sub> sorption isotherms of 4–6 were collected at 273 and 298 K and did not transform to their more open phases (Figure S13). The isosteric heat of adsorption ( $Q_{st}$ ) of 5 for CO<sub>2</sub> was calculated from its 273 and 298 K isotherms to be 21.5 kJ/mol (Figure S14). With respect to the desorption branches of the isotherms, the flexible materials 4, 5, and 6 exhibited various degrees of hysteresis, while there was no hysteresis for 1–3. The difference in the sorption profiles of 1–3 vs 4–6 is illustrated by the differences between arbitrary working capacities of CO<sub>2</sub> at 195 K calculated between 0.1 and 1 bar. The values for 1 (70 cm<sup>3</sup>/g), 2 (69 cm<sup>3</sup>/g), and 3 (62

cm<sup>3</sup>/g) are reduced due to their Type-I uptake characteristics compared to those for 4 (70 cm<sup>3</sup>/g), 5 (174 cm<sup>3</sup>/g), and 6 (154 cm<sup>3</sup>/g), which show flexible isotherms. Grand canonical Monte Carlo simulations of the inclusion of CO<sub>2</sub> by the porous phases of 4–6 suggest no specific binding sites between the CO<sub>2</sub> molecules and pore walls (Figure S15). Significant N<sub>2</sub> uptake was found only in 2 (37 cm<sup>3</sup>/g), whereas the other five materials exhibited negligible uptake (Figure S16). The negligible N<sub>2</sub> uptakes of 1 and 3 can be attributed to their small pore size (Figure S17). For 4–6, there is negligible N<sub>2</sub> uptake, because transformation to their phases cannot be triggered by N<sub>2</sub>.

**Conclusion.** We report a family of six **sql** CNs with interdigitated bilayer packing and different lengths and bulkiness of pendent groups in their ia linkers. Upon desolvation and gas sorption, those CNs with short but bulkier or longer pendent groups exhibited structural transformations between low-porosity phases and high-porosity phases facilitated by both interlayer expansion and linker hinge-like motions. While **sql** layer expansion dominated for 4 (short and bulky pendent moiety), linker hinge-like motion dominated for 5 and 6 (longer pendent groups), as revealed by SCXRD and VT-PXRD experiments. In addition, whereas Type F–II and F–IV CO<sub>2</sub> sorption isotherms were observed in the flexible **sql** CNs (4–6), those with smaller pendent groups exhibited rigid structures and Type I CO<sub>2</sub> sorption isotherms (1, 2, and 3). That the stimulus-induced properties of 1–6 were so profoundly influenced by the systematic substitution of pendent groups offers a platform for exploring the development of sorbents with structural flexibility.

## ■ ASSOCIATED CONTENT

### Supporting Information

The Supporting Information is available free of charge at <https://pubs.acs.org/doi/10.1021/acsmaterialslett.3c00565>.

Materials and methods, supporting figures, supporting tables, and supporting references (PDF)

X-ray data for [Zn(mia)(bphy)]<sub>n</sub> (2) (CIF)  
 X-ray data for [Zn(moia)(bphy)]<sub>n</sub> (3) (CIF)  
 X-ray data for [Zn(tbia)(bphy)]<sub>n</sub> (4- $\alpha$ ) (CIF)  
 X-ray data for [Zn(tbia)(bphy)]<sub>n</sub> (4- $\alpha'$ ) (CIF)  
 X-ray data for [Zn(tbia)(bphy)]<sub>n</sub> (4- $\beta$ ) (CIF)  
 X-ray data for [Zn(pdia)(bphy)]<sub>n</sub> (5- $\alpha$ ) (CIF)  
 X-ray data for [Zn(dpdi)(bphy)]<sub>n</sub> (6- $\alpha$ ) (CIF)  
 X-ray data for [Zn(dpdi)(bphy)]<sub>n</sub> (6- $\beta$ ) (CIF)

## AUTHOR INFORMATION

### Corresponding Author

Michael J. Zaworotko – Department of Chemical Science, Bernal Institute, University of Limerick, Limerick V94 T9PX, Republic of Ireland; [orcid.org/0000-0002-1360-540X](https://orcid.org/0000-0002-1360-540X); Email: [Michael.Zaworotko@ul.ie](mailto:Michael.Zaworotko@ul.ie)

### Authors

Xia Li – Department of Chemical Science, Bernal Institute, University of Limerick, Limerick V94 T9PX, Republic of Ireland

Debroto Sensharma – Department of Chemical Science, Bernal Institute, University of Limerick, Limerick V94 T9PX, Republic of Ireland; [orcid.org/0000-0002-4918-0730](https://orcid.org/0000-0002-4918-0730)

Kyriaki Koupepidou – Department of Chemical Science, Bernal Institute, University of Limerick, Limerick V94 T9PX, Republic of Ireland

Xiang-Jing Kong – Department of Chemical Science, Bernal Institute, University of Limerick, Limerick V94 T9PX, Republic of Ireland; [orcid.org/0000-0003-2940-8600](https://orcid.org/0000-0003-2940-8600)

Complete contact information is available at:

<https://pubs.acs.org/10.1021/acsmaterialslett.3c00565>

### Author Contributions

The manuscript was written through contributions of all authors. All authors have given approval to the final version of the manuscript. CRediT: Xia Li conceptualization, investigation, methodology, writing-original draft, writing-review & editing; Debroto Sensharma methodology, writing-review & editing; Kyriaki Koupepidou methodology, writing-review & editing; Xiang-Jing Kong methodology, writing-review & editing; Michael J. Zaworotko conceptualization, formal analysis, writing-original draft, writing-review & editing.

### Funding

We gratefully acknowledge Science Foundation Ireland (SFI Awards 16/IA/4624), the Irish Research Council (IRCLA/2019/167), the European Research Council (ADG 885695).

### Notes

The authors declare no competing financial interest.

## ACKNOWLEDGMENTS

The authors gratefully acknowledge advice given by Dr. Mei-Yan Gao, Chenghua Deng, and Dr. Alan Eaby from University of Limerick. We also thank Dr. Yun-Lei Peng from China University of Petroleum.

## REFERENCES

- (1) Férey, G.; Serre, C. Large Breathing Effects in Three-Dimensional Porous Hybrid Matter: Facts, Analyses, Rules and Consequences. *Chem. Soc. Rev.* **2009**, *38* (5), 1380–1399.
- (2) Peh, S. B.; Karmakar, A.; Zhao, D. Multiscale Design of Flexible Metal–Organic Frameworks. *Trends Chem.* **2020**, *2* (3), 199–213.
- (3) Wang, S. Q.; Mukherjee, S.; Zaworotko, M. J. Spiers Memorial Lecture: Coordination Networks That Switch between Nonporous and Porous Structures: An Emerging Class of Soft Porous Crystals. *Faraday Discuss.* **2021**, *231*, 9–50.
- (4) Behera, N.; Duan, J.; Jin, W.; Kitagawa, S. The Chemistry and Applications of Flexible Porous Coordination Polymers. *EnergyChem.* **2021**, *3* (6), No. 100067.
- (5) Zhao, P.; Tsang, S. C. E.; Fairen-Jimenez, D. Structural Heterogeneity and Dynamics in Flexible Metal–Organic Frameworks. *Cell Reports Phys. Sci.* **2021**, *2* (9), No. 100544.
- (6) O’Hearn, D. J.; Bajpai, A.; Zaworotko, M. J. The “Chemistree” of Porous Coordination Networks: Taxonomic Classification of Porous Solids to Guide Crystal Engineering Studies. *Small* **2021**, *17* (22), No. 2006351.
- (7) Janiak, C.; Vieth, J. K. MOFs, MILs and More: Concepts, Properties and Applications for Porous Coordination Networks (PCNs). *New J. Chem.* **2010**, *34* (11), 2366–2388.
- (8) Schneemann, A.; Bon, V.; Schwedler, I.; Senkovska, I.; Kaskel, S.; Fischer, R. A. Flexible Metal–Organic Frameworks. *Chem. Soc. Rev.* **2014**, *43* (16), 6062–6096.
- (9) Deria, P.; Gómez-Gualdrón, D. A.; Bury, W.; Schaefer, H. T.; Wang, T. C.; Thallapally, P. K.; Sarjeant, A. A.; Snurr, R. Q.; Hupp, J. T.; Farha, O. K. Ultraporos, Water Stable, and Breathing Zirconium-Based Metal–Organic Frameworks with Ftw Topology. *J. Am. Chem. Soc.* **2015**, *137* (40), 13183–13190.
- (10) Gao, S.; Morris, C. G.; Lu, Z.; Yan, Y.; Godfrey, H. G. W.; Murray, C.; Tang, C. C.; Thomas, K. M.; Yang, S.; Schröder, M. Selective Hysteretic Sorption of Light Hydrocarbons in a Flexible Metal–Organic Framework Material. *Chem. Mater.* **2016**, *28* (7), 2331–2340.
- (11) Mason, J. A.; Oktawiec, J.; Taylor, M. K.; Hudson, M. R.; Rodriguez, J.; Bachman, J. E.; Gonzalez, M. I.; Cervellino, A.; Guagliardi, A.; Brown, C. M.; Llewellyn, P. L.; Masciocchi, N.; Long, J. R. Methane Storage in Flexible Metal–Organic Frameworks with Intrinsic Thermal Management. *Nature* **2015**, *527* (7578), 357–361.
- (12) Koupepidou, K.; Nikolayenko, V. I.; Sensharma, D.; Bezrukov, A. A.; Vandichel, M.; Nikkhah, S. J.; Castell, D. C.; Oyekan, K. A.; Kumar, N.; Subanbekova, A.; Vandenberghe, W. G.; Tan, K.; Barbour, L. J.; Zaworotko, M. J. One Atom Can Make All the Difference: Gas-Induced Phase Transformations in Bisimidazole-Linked Diamondoid Coordination Networks. *J. Am. Chem. Soc.* **2023**, *145*, 10197.
- (13) Matsuda, R.; Kitaura, R.; Kitagawa, S.; Kubota, Y.; Belosludov, R. V.; Kobayashi, T. C.; Sakamoto, H.; Chiba, T.; Takata, M.; Kawazoe, Y.; Mita, Y. Highly Controlled Acetylene Accommodation in a Metal–Organic Microporous Material. *Nature* **2005**, *436* (7048), 238–241.
- (14) Shivanna, M.; Otake, K.; Song, B.-Q.; van Wyk, L. M.; Yang, Q.-Y.; Kumar, N.; Feldmann, W. K.; Pham, T.; Suepaul, S.; Space, B.; Barbour, L. J.; Kitagawa, S.; Zaworotko, M. J. Benchmark Acetylene Binding Affinity and Separation through Induced Fit in a Flexible Hybrid Ultramicroporous Material. *Angew. Chem., Int. Ed.* **2021**, *60* (37), 20383–20390.
- (15) Dong, Q.; Huang, Y.; Hyeon-Deuk, K.; Chang, I.-Y.; Wan, J.; Chen, C.; Duan, J.; Jin, W.; Kitagawa, S. Shape- and Size-Dependent Kinetic Ethylene Sieving from a Ternary Mixture by a Trap-and-Flow Channel Crystal (Adv. Funct. Mater. 38/2022). *Adv. Funct. Mater.* **2022**, *32* (38), No. 2270212.
- (16) Wang, S. Q.; Mukherjee, S.; Patyk-Kaźmierczak, E.; Darwish, S.; Bajpai, A.; Yang, Q. Y.; Zaworotko, M. J. Highly Selective, High-Capacity Separation of o-Xylene from C8 Aromatics by a Switching Adsorbent Layered Material. *Angew. Chem., Int. Ed.* **2019**, *58* (20), 6630–6634.
- (17) Roztocki, K.; Formalik, F.; Krawczuk, A.; Senkovska, I.; Kuchta, B.; Kaskel, S.; Matoga, D. Collective Breathing in an Eightfold Interpenetrated Metal–Organic Framework: From Mechanistic Understanding towards Threshold Sensing Architectures. *Angew. Chem., Int. Ed.* **2020**, *59* (11), 4491–4497.
- (18) Li, X.; Sensharma, D.; Nikolayenko, V. I.; Darwish, S.; Bezrukov, A. A.; Kumar, N.; Liu, W.; Kong, X.-J.; Zhang, Z.

Zaworotko, M. J. Structural Phase Transformations Induced by Guest Molecules in a Nickel-Based 2D Square Lattice Coordination Network. *Chem. Mater.* **2023**, *35* (2), 783–791.

(19) Moghadam, P. Z.; Li, A.; Liu, X.-W.; Bueno-Perez, R.; Wang, S.-D.; Wiggin, S. B.; Wood, P. A.; Fairen-Jimenez, D. Targeted Classification of Metal–Organic Frameworks in the Cambridge Structural Database (CSD). *Chem. Sci.* **2020**, *11* (32), 8373–8387.

(20) Chen, B.; Liang, C.; Yang, J.; Contreras, D. S.; Clancy, Y. L.; Lobkovsky, E. B.; Yaghi, O. M.; Dai, S. A Microporous Metal–Organic Framework for Gas-Chromatographic Separation of Alkanes. *Angew. Chem., Int. Ed.* **2006**, *45* (9), 1390–1393.

(21) Serre, C.; Mellot-Draznieks, C.; Surblé, S.; Audebrand, N.; Filinchuk, Y.; Férey, G. Role of Solvent-Host Interactions That Lead to Very Large Swelling of Hybrid Frameworks. *Science*. **2007**, *315* (5820), 1828–1831.

(22) Yang, Q. Y.; Lama, P.; Sen, S.; Lusi, M.; Chen, K. J.; Gao, W. Y.; Shivanna, M.; Pham, T.; Hosono, N.; Kusaka, S.; Perry, J. J.; Ma, S.; Space, B.; Barbour, L. J.; Kitagawa, S.; Zaworotko, M. J. Reversible Switching between Highly Porous and Nonporous Phases of an Interpenetrated Diamondoid Coordination Network That Exhibits Gate-Opening at Methane Storage Pressures. *Angew. Chem., Int. Ed.* **2018**, *57* (20), 5684–5689.

(23) Sakata, Y.; Furukawa, S.; Kondo, M.; Hirai, K.; Horike, N.; Takashima, Y.; Uehara, H.; Louvain, N.; Meilikhov, M.; Tsuruoka, T.; Isoda, S.; Kosaka, W.; Sakata, O.; Kitagawa, S. Shape-Memory Nanopores Induced in Coordination Frameworks by Crystal Downsizing. *Science*. **2013**, *339* (6116), 193–196.

(24) Gardner, G. B.; Venkataraman, D.; Moore, J. S.; Lee, S. Spontaneous assembly of a hinged coordination network. *Nature*. **1995**, *374*, 792–795.

(25) Mellot-Draznieks, C.; Serre, C.; Surblé, S.; Audebrand, N.; Férey, G. Very Large Swelling in Hybrid Frameworks: A Combined Computational and Powder Diffraction Study. *J. Am. Chem. Soc.* **2005**, *127* (46), 16273–16278.

(26) Bon, V.; Klein, N.; Senkovska, I.; Heerwig, A.; Getzschmann, J.; Wallacher, D.; Zizak, I.; Brzhezinskaya, M.; Mueller, U.; Kaskel, S. Exceptional Adsorption-Induced Cluster and Network Deformation in the Flexible Metal–Organic Framework DUT-8(Ni) Observed by in Situ X-Ray Diffraction and EXAFS. *Phys. Chem. Chem. Phys.* **2015**, *17* (26), 17471–17479.

(27) Seo, J.; Bonneau, C.; Matsuda, R.; Takata, M.; Kitagawa, S. Soft Secondary Building Unit: Dynamic Bond Rearrangement on Multinuclear Core of Porous Coordination Polymers in Gas Media. *J. Am. Chem. Soc.* **2011**, *133* (23), 9005–9013.

(28) Hiraide, S.; Tanaka, H.; Ishikawa, N.; Miyahara, M. T. Intrinsic Thermal Management Capabilities of Flexible Metal–Organic Frameworks for Carbon Dioxide Separation and Capture. *ACS Appl. Mater. Interfaces* **2017**, *9* (46), 41066–41077.

(29) Zhu, A.-X.; Yang, Q.-Y.; Kumar, A.; Crowley, C.; Mukherjee, S.; Chen, K.-J.; Wang, S.-Q.; O’Nolan, D.; Shivanna, M.; Zaworotko, M. J. Coordination Network That Reversibly Switches between Two Nonporous Polymorphs and a High Surface Area Porous Phase. *J. Am. Chem. Soc.* **2018**, *140* (46), 15572–15576.

(30) Park, J.; Yuan, D.; Pham, K. T.; Li, J.-R.; Yakovenko, A.; Zhou, H.-C. Reversible Alteration of CO<sub>2</sub> Adsorption upon Photochemical or Thermal Treatment in a Metal–Organic Framework. *J. Am. Chem. Soc.* **2012**, *134* (1), 99–102.

(31) Lyndon, R.; Konstas, K.; Ladewig, B. P.; Southon, P. D.; Kepert, P. C. J.; Hill, M. R. Dynamic Photo-Switching in Metal–Organic Frameworks as a Route to Low-Energy Carbon Dioxide Capture and Release. *Angew. Chem., Int. Ed.* **2013**, *52* (13), 3695–3698.

(32) Castell, D. C.; Nikolayenko, V. I.; Sensharma, D.; Koupepidou, K.; Forrest, K. A.; Solanilla-Salinas, C. J.; Space, B.; Barbour, L. J.; Zaworotko, M. J. Crystal Engineering of Two Light and Pressure Responsive Physisorbents. *Angew. Chem., Int. Ed.* **2023**, *62*, No. e202219039.

(33) Kondo, A.; Noguchi, H.; Ohnishi, S.; Kajiro, H.; Tohdoh, A.; Hattori, Y.; Xu, W.-C.; Tanaka, H.; Kanoh, H.; Kaneko, K. Novel

Expansion/Shrinkage Modulation of 2D Layered MOF Triggered by Clathrate Formation with CO<sub>2</sub> Molecules. *Nano Lett.* **2006**, *6* (11), 2581–2584.

(34) Llewellyn, P. L.; Horcajada, P.; Maurin, G.; Devic, T.; Rosenbach, N.; Bourrelly, S.; Serre, C.; Vincent, D.; Loera-Serna, S.; Filinchuk, Y.; Férey, G. Complex Adsorption of Short Linear Alkanes in the Flexible Metal–Organic–Framework MIL-53(Fe). *J. Am. Chem. Soc.* **2009**, *131* (50), 13002–13008.

(35) Henke, S.; Schneemann, A.; Fischer, R. A. Massive Anisotropic Thermal Expansion and Thermo-Responsive Breathing in Metal–Organic Frameworks Modulated by Linker Functionalization. *Adv. Funct. Mater.* **2013**, *23* (48), 5990–5996.

(36) Bezuidenhout, C. X.; Smith, V. J.; Esterhuysen, C.; Barbour, L. J. Solvent- and Pressure-Induced Phase Changes in Two 3D Copper Glutarate-based Metal–Organic Frameworks via Glutarate (+gauche  $\rightleftharpoons$  -gauche) Conformational Isomerism. *J. Am. Chem. Soc.* **2017**, *139* (16), 5923–5929.

(37) Wang, J.; Zhang, Y.; Zhang, P.; Hu, J.; Lin, R. B.; Deng, Q.; Zeng, Z.; Xing, H.; Deng, S.; Chen, B. Optimizing Pore Space for Flexible-Robust Metal–Organic Framework to Boost Trace Acetylene Removal. *J. Am. Chem. Soc.* **2020**, *142* (21), 9744–9751.

(38) Krause, S.; Bon, V.; Senkovska, I.; Stoeck, U.; Wallacher, D.; Többs, D. M.; Zander, S.; Pillai, R. S.; Maurin, G.; Coudert, F. X.; Kaskel, S. A Pressure-Amplifying Framework Material with Negative Gas Adsorption Transitions. *Nature* **2016**, *532* (7599), 348–352.

(39) Krause, S.; Evans, J. D.; Bon, V.; Senkovska, I.; Iacomi, P.; Kolbe, F.; Ehrling, S.; Troschke, E.; Getzschmann, J.; Többs, D. M.; Franz, A.; Wallacher, D.; Yot, P. G.; Maurin, G.; Brunner, E.; Llewellyn, P. L.; Coudert, F. X.; Kaskel, S. Towards General Network Architecture Design Criteria for Negative Gas Adsorption Transitions in Ultraporos Frameworks. *Nat. Commun.* **2019**, *10* (1), 3632.

(40) Wang, Z.; Cohen, S. M. Modulating Metal–Organic Frameworks to Breathe: A Postsynthetic Covalent Modification Approach. *J. Am. Chem. Soc.* **2009**, *131* (46), 16675–16677.

(41) He, Y.; Shang, J.; Gu, Q.; Li, G.; Li, J.; Singh, R.; Xiao, P.; Webley, P. A. Converting 3D Rigid Metal–Organic Frameworks (MOFs) to 2D Flexible Networks via Ligand Exchange for Enhanced CO<sub>2</sub>/N<sub>2</sub> and CH<sub>4</sub>/N<sub>2</sub> Separation. *Chem. Commun.* **2015**, *51* (79), 14716–14719.

(42) Wieme, J.; Vanduyffhuys, L.; Rogge, S. M. J.; Waroquier, M.; Van Speybroeck, V. Exploring the Flexibility of MIL-47(V)-Type Materials Using Force Field Molecular Dynamics Simulations. *J. Phys. Chem. C* **2016**, *120* (27), 14934–14947.

(43) Biswas, S.; Ahnfeldt, T.; Stock, N. New Functionalized Flexible Al-MIL-53-X (X = -Cl, -Br, -CH<sub>3</sub>, -NO<sub>2</sub>, -(OH)<sub>2</sub>) Solids: Syntheses, Characterization, Sorption, and Breathing Behavior. *Inorg. Chem.* **2011**, *50* (19), 9518–9526.

(44) Devic, T.; Horcajada, P.; Serre, C.; Salles, F.; Maurin, G.; Moulin, B.; Heurtaux, D.; Clet, G.; Vimont, A.; Grenèche, J.-M.; Ouay, B. L.; Moreau, F.; Magnier, E.; Filinchuk, Y.; Marrot, J.; Lavalley, J.-C.; Daturi, M.; Férey, G. Functionalization in Flexible Porous Solids: Effects on the Pore Opening and the Host–Guest Interactions. *J. Am. Chem. Soc.* **2010**, *132* (3), 1127–1136.

(45) Wang, G.; Leus, K.; Couck, S.; Tack, P.; Depauw, H.; Liu, Y.-Y.; Vincze, L.; Denayer, J. F. M.; Van Der Voort, P. Enhanced Gas Sorption and Breathing Properties of the New Sulfone Functionalized COMOC-2 Metal Organic Framework. *Dalton Trans.* **2016**, *45* (23), 9485–9491.

(46) Li, D.; Kaneko, K. Hydrogen Bond-Regulated Microporous Nature of Copper Complex-Assembled Microcrystals. *Chem. Phys. Lett.* **2001**, *335* (1), 50–56.

(47) Kondo, A.; Noguchi, H.; Carlucci, L.; Proserpio, D. M.; Ciani, G.; Kajiro, H.; Ohba, T.; Kanoh, H.; Kaneko, K. Double - Step Gas Sorption of a Two - Dimensional Metal - Organic Framework. *J. Am. Chem. Soc.* **2007**, *129* (41), 12362–12363.

(48) Kanoh, H.; Kondo, A.; Noguchi, H.; Kajiro, H.; Tohdoh, A.; Hattori, Y.; Xu, W.-C.; Inoue, M.; Sugiura, T.; Morita, K.; Tanaka, H.; Ohba, T.; Kaneko, K. Elastic Layer-Structured Metal Organic Frameworks (ELMs). *J. Colloid Interface Sci.* **2009**, *334* (1), 1–7.

(49) Ichikawa, M.; Kondo, A.; Noguchi, H.; Kojima, N.; Ohba, T.; Kajiro, H.; Hattori, Y.; Kanoh, H. Double-Step Gate Phenomenon in CO<sub>2</sub> Sorption of an Elastic Layer-Structured MOF. *Langmuir* **2016**, *32* (38), 9722–9726.

(50) Liu, X. M.; Lin, R. B.; Zhang, J. P.; Chen, X. M. Low-dimensional porous coordination polymers based on 1, 2-bis (4-pyridyl) hydrazine: from structure diversity to ultrahigh CO<sub>2</sub>/CH<sub>4</sub> selectivity. *Inorg. Chem.* **2012**, *51* (10), 5686–5692.

(51) Groom, C. R.; Bruno, I. J.; Lightfoot, M. P.; Ward, S. C. *Acta Crystallogr., Sect. B Struct. Sci., Cryst. Eng. Mater.* **2016**, *72*, 171.

(52) Shimao, I.; Oae, S. The Wallach Rearrangement of Some 4,4'-Disubstituted Azoxybenzenes. *Bull. Chem. Soc. Jpn.* **1983**, *56* (2), 643–644.

(53) Park, J.; Sun, L.-B.; Chen, Y.-P.; Perry, Z.; Zhou, H.-C. Azobenzene-Functionalized Metal–Organic Polyhedra for the Optically Responsive Capture and Release of Guest Molecules. *Angew. Chem., Int. Ed.* **2014**, *53* (23), 5842–5846.

(54) Dinker, M. K.; Zhao, K.; Dai, Z.; Ding, L.; Liu, X.-Q.; Sun, L.-B. Porous Liquids Responsive to Light\*\*. *Angew. Chem., Int. Ed.* **2022**, *61* (50), No. e202212326.

(55) Liu, X.-M.; Xie, L.-H.; Lin, J.-B.; Lin, R.-B.; Zhang, J.-P.; Chen, X.-M. Flexible Porous Coordination Polymers Constructed from 1,2-Bis(4-Pyridyl) Hydrazine via Solvothermal in Situ Reduction of 4,4'-Azopyridine. *Dalton Trans.* **2011**, *40* (34), 8549–8554.

(56) Abrahams, J. P.; Leslie, A. G. W. Methods Used in the Structure Determination of Bovine Mitochondrial F1 ATPase. *Acta Crystallogr. Sect. D* **1996**, *52* (1), 30–42.

(57) Spek, A. L. Single-Crystal Structure Validation with the Program PLATON. *J. Appl. Crystallogr.* **2003**, *36* (1), 7–13.

(58) Islamoglu, T.; Idrees, K. B.; Son, F. A.; Chen, Z.; Lee, S.-J.; Li, P.; Farha, O. K. Are You Using the Right Probe Molecules for Assessing the Textural Properties of Metal–Organic Frameworks? *J. Mater. Chem. A* **2021**, *10* (1), 157–173.